A molecular dynamics and finite elements study of nanoscale thermal contact conductance

G. Anciaux*, J.F. Molinari

[a] *Ecole Polytechnique Fédérale de Lausanne (EPFL)*
Faculté ENAC-IIC, Computational Solid Mechanics Laboratory (lsms.epfl.ch/)
CH-1015 Lausanne, Switzerland

Abstract

We study scale effects on the conductivity of crystalline contacting interfaces. The approach focuses on the role played by lattice vibrations in the thermal conductivity using finite elements and molecular dynamics models. A special effort is made at calibrating the continuum model directly from molecular dynamics simulations. An innovative method that uses the temperature evolution issued from an impulse boundary condition is employed to compute heat conductivity, which is notoriously known as difficult to measure. Using this approach, a parametric study is conducted on a set of contacting surfaces on which we specify asperities wavelengths. It is shown that the usual power laws that relate contact area ratio with thermal conductivity do not apply at the nanoscale.

Keywords: Heat, thermal conductance, molecular dynamics, finite elements, Fourier conduction, ballistic conduction.

1. Introduction

For many engineering applications, the thermal conductivity of an object having an internal interface is of paramount importance. For instance, the current trend for miniaturization brings the need for nanoscale cooling systems [1], which calls for a good knowledge of the thermal contact conductance from the heat source to the heat regulator.

Machined, fractured, and even polished surfaces all seem to follow the general description of fractal surfaces with parametrized power spectrum density [2–4]. Furthermore, the surface topology of the contact interface between two solids strongly alters the contact conductance. Thus the interface properties can be deduced from contact conductance measures and reversely surface properties can be chosen to tune the conductivity. Experimentally, a conductance power law is observed, which writes $\kappa \propto p^{\beta}$ with κ the conductance, p the applied pressure, and β an exponent [5–7]. These laws found applications in several macroscale finite elements studies [8, 9].

Several theories and numerical simulations justifying this correlation exist. One of these modeling approaches, as developed in [10–16], uses the parallel existing between

*Corresponding author: guillaume.anciaux@epfl.ch

elastic deformation theory and diffusion equation (heat/electrical conduction) to derive a relation of proportionality between the incremental stiffness at the surface and the conductance. It takes the form of the relation $\kappa \propto \frac{\partial p}{\partial d}$ with d the mean separation at the contacting interface. This pressure/stiffness variation depends on the mechanical interface deformations in response to loading [17–20] and helps to recover the power law relating pressure and contact conductance. Differences amongst theories stand on the approach used to derive the mechanics of the contact rather than the conductivity problem itself. This assumes that every contacting asperity contributes to the global conductivity according to their contact area, which does not take into account possible heat transport interactions between asperities.

Even though this is certainly acceptable at macroscopic scales, when going down to the atomic scale the discreteness of matter leads to a ballistic phonon heat transport [21–23]. Phonons are quantum of lattice vibrations, which are quantized because of small distances to boundaries or low temperatures. Some phonons of low frequency admit an important mean free path - especially in pristine crystalline materials - unless an obstacle is introduced. This means that the energy transport is not following the classical Fourier heat equation but rather a classical wave equation. Thus the heat flow will be perturbed when the geometry implies short distances between free boundaries. A surface topology displaying small wavelengths clearly falls in that condition. This phonon scattering effect has been studied experimentally, theoretically and in numerical simulations [24–32]. However, simple geometries were considered in the theories, and numerical studies rarely included the presence of defects.

Classical molecular dynamics can qualitatively catch the lattice vibration contribution in the heat conduction. To the best of our knowledge, there are only two classes of methods that can be used to measure the heat conductivity within MD simulations. The first relies on the Green-Kubo statistical relation to extract the conductance from an entire group of atoms supposed at equilibrium [33]. This is quite accurate but the equilibrium assumption must be fulfilled and renders difficult the introduction of localized defects. Non equilibrium molecular dynamics [34] belongs to the second class. It imposes a heat flux that brings a temperature gradient. The ratio of the flux to the induced temperature gradient is a measure of the thermal conductivity. Unfortunately, temperature gradients obtained with this method are perturbed when defects are introduced. This motivates a new approach to extract thermal conductance from material samples with a customized defect profile.

The objective of this work is to describe scale effects on crystalline-material conductivity by comparing continuum (finite elements) and molecular dynamics simulations. This scale effect is directed toward contact conductance by introducing an interface with a topology involving a single wavelength. This will be achieved within three parts. In a first section we present our numerical models. The Fourier heat equation and the finite-element model will be briefly introduced. Then an important effort will be done in describing the molecular settings and especially the methods used to extract physical constants. In a second part, we introduce a new procedure that is aimed at extracting thermal conductance when defects are present in the material. This technique, which uses the predicted response to a temperature impulse, will be described and validated against Green-Kubo predictions but also against finite elements computations. The third part introduces contacting interfaces as the base of a parametric study. From that study, the relation between contacting area and conductance will be presented for both atomic

and macroscopic scales. We conclude with a discussion and contrast our results with power-laws observed at the macroscale.

Nomenclature

k	Thermal conductivity
α	Thermal diffusivity
ϵ	Lennard Jones energy parameter
α_L	Linear thermal expansion coefficient
α_V	Volumique thermal expansion coefficient
$\mathbf{J}$	Global energy flux
$\mathbf{S}_i$	Stress tensor computed on atom i
$\mathbf{v}_i$	Velocity of atom i
ϕ	Lennard Jones potential function
ρ	Mass density
σ	Lennard Jones distance parameter, the atomic radius
a	Face cubic centered lattice dimension
c_v	Heat capacity at constant volume per unit of mass
e_i	Energy of atom i
k_b	Boltzmann constant
m	Atomic mass
T	Temperature
V_i	Current volume surrounding atom i

2. Numerical models

The purpose of this section is to describe the modeling properties of the continuum and atomic scale models. At the continuum level the heat transport follows the Fourier heat equation taking the form:

$$\rho c_v \dot{T} = -k\nabla^2 T \tag{1}$$

where ρ is the density of the solid considered, c_v is the mass specific heat capacity at constant volume and T is the temperature scalar field. The heat equation above has no volumetric heat generation term since we will not consider this kind of energy input in our study. The numerical continuum models will all use an unstructured mesh and an explicit integration scheme applied to a lumped [35, 36] heat capacity approximation of (1). To be able to compare this continuum description of heat transport to atomic scale simulations, the physical constants should be calculated directly using molecular dynamics simulations.

All our molecular dynamics simulations will consider a generic material for which the initial state is a perfect crystal with a face centered cubic (FCC) lattice with dimension a ($a_0 = 4.032$ Å for ground state). The mass of each atom is set to $m = 26.98$ g/mol. The inter-atomic potential used to drive atoms is the *Lennard Jones* potential [37, 38]. The expression of the associated global potential energy is:

$$E_{tot} = \frac{1}{2}\sum_{i,j\neq i}\phi(r_{ij}) \qquad with \qquad \phi(r) = \epsilon\left(\left(\frac{\sigma}{r}\right)^{12} - \left(\frac{\sigma}{r}\right)^{6}\right) \tag{2}$$

where $\sigma = 2.596$ Å and $\epsilon = 2.4621$ kcal/mol have been computed to fit a Young's modulus of 68 GPa and a Poisson ratio of ~ 0.3. The cutoff radius has been chosen as $r_{cut} = 6.039$ Å so that atoms interact up to their fourth neighbors. More details are available within [39] for the derivation of Lennard Jones parameters from Young's modulus and Poisson ratio. Using this description of the atomic interactions, the physical constants relevant to the continuum analogy, mass density, heat capacity and heat conductivity, are computed in the following section.

2.1. Mass density and thermal expansion

A FCC crystal with the lattice constant $a(T)$ will have a mass density given by the formula:

$$\rho(T) = \frac{4m}{a(T)^3} = (1+\alpha_L T)^{-3}\,\frac{4m}{a_0^3} = (1+\alpha_L T)^{-3}\,\rho_0 \tag{3}$$

where m is the atomic mass. $a(T)$ admits a temperature dependence resulting from the thermal expansion $\alpha_L(T)$. We monitored the volume expansion as a function of temperature in an isothermal-isobarc enemble (NPT) . The result is the lattice parameter versus temperature evolution presented on figure 1. At ground state the density is $\rho_0 \simeq 1.65$ g/mol/Å^3. At 100 K the thermal expansion is $\alpha_L(100) \simeq 0.00396$ K^{-1} and the density thus computed is $\rho(100) \simeq 1.627$ g/mol/Å^3.

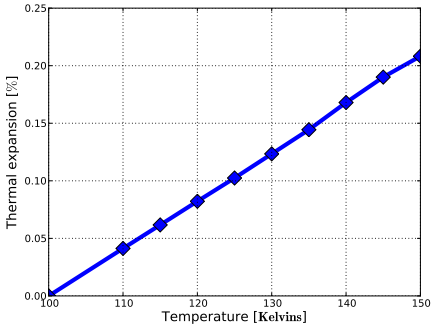

Figure 1: MD measure of the relative increase in the equilibrium lattice size with respect to temperature. The expansion factor is the slope of this curve, which is constant in the range $100 - 150$ Kelvins.

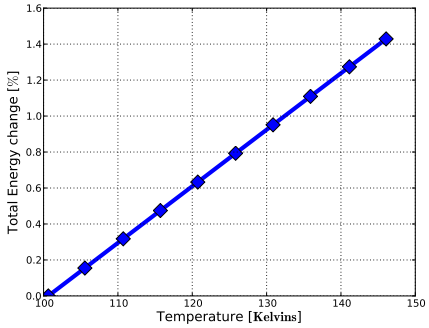

Figure 2: MD measure of the variation of total energy with respect to temperature. The heat capacity is the slope of that curve which is constant in the range between 100 to 150 Kelvins.

2.2. Heat capacity

The mass specific heat capacity can be computed as the variation of total energy with respect to a change of temperature at constant volume. Figure 2 presents the curve obtained during such a simulation on a cubic box. The observable linear relation states that the heat capacity remains constant in the range of temperatures we wish to treat in the present work (100 - 150 Kelvins). This allows to provide the engineering parameter $c_v(100) \simeq 2.18987 \cdot 10^{-4}$ kcal/g/K. Several simulations of various sizes where performed (but not presented here) that show that the measured capacity does not depend strongly on the domain size when at least a decade of atoms is considered.

2.3. Heat conductivity

Last but not least is the conductivity parameter. As stated in the introduction many paths can be found in the literature in order to extract such a coefficient from molecular simulations. Among them, the Green-Kubo statistics [33] method and the Non Equilibrium Molecular Dynamics (NEMD) [34] are well-established tools in the case of homogeneous material. The advantage of the Green-Kubo relation is that it connects the transport coefficients to the auto-correlation of the energy flux fluctuations at equilibrium and this for any triggered temperature. The drawback stands in the fact that the domain must be homogeneous and at an equilibrated state. Also fairly long simulations have to be made for getting convergence of the auto-correlation functions. Nevertheless, in order to define the settings of our model, the approach is well suited since we can choose precisely the temperature at which we seek the heat conductivity. For the calibration of our constants we conducted two molecular dynamics simulations, one at 100 K, the other at 150 K. The simulations consist of a cubic box containing 256 atoms with periodic boundary conditions. The global energy flux vector is defined as [40]:

$$\mathbf{J} = \frac{1}{V}\left[\sum_i e_i \mathbf{v_i} - \sum_i \mathbf{S}_i V_i \mathbf{v_i}\right] \tag{4}$$

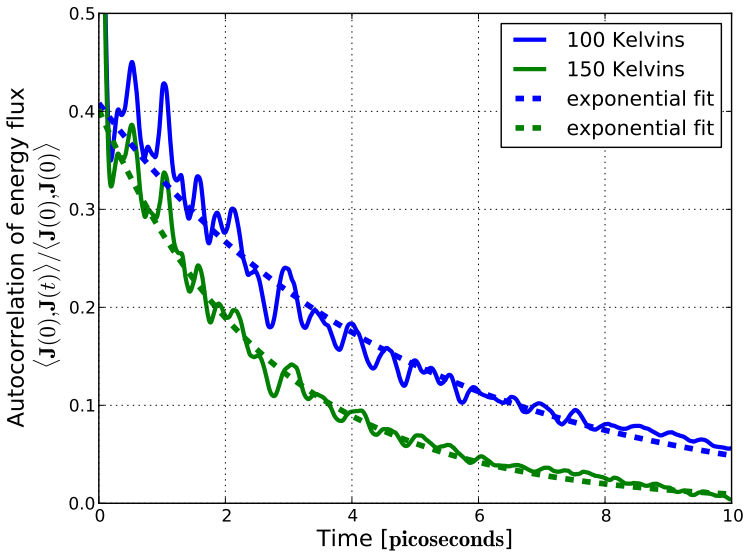

Figure 3: Auto-correlation of the energy flux with respect to time at temperatures 100 and 150 Kelvins. The exponential trends are also provided by the dashed lines.

where V is the volume of the system, V_i, e_i, $\mathbf{v_i}$ and S_i are per-atom quantities, respectively volume, energy, velocity and stress tensor. The Green-Kubo relation is:

$$k = \frac{V}{k_b T^2} \int_0^\infty \langle \mathbf{J}(0), \mathbf{J}(t) \rangle dt \tag{5}$$

where k_b is the Boltzmann constant and the angular brackets stand for time averaging. Figure 3 presents the time-averaged auto-correlation function $\langle \mathbf{J}(0), \mathbf{J}(t) \rangle$ for the two simulations. As can be seen, the global behavior can be approximated with an exponential function. Thus the integral of equation (5) can be computed semi-analytically and it gives the values $k_{100} = 3 \cdot 10^{-4}$ kcal/mol/(fs $\cdot$ Å $\cdot$ K) and $k_{150} = 1.9 \cdot 10^{-4}$ kcal/mol/(fs $\cdot$ Å $\cdot$ K) which corresponds in more usual units to $k_{100} = 20$ W/m/K and $k_{150} = 13.1$ W/m/K. It is worth noticing that the computed conductivities are small when compared to metallic systems. Indeed in these molecular dynamics simulations, the electronic contribution to conduction is not part of the model, thus leading to small conduction values. For the purpose of the present study, which aims at comparing atomistic and continuum scales for phonon conduction, the generic material that has been defined allows us to ignore this point.

In this section we have computed the constants of the Fourier continuum model of the diffusion equation (1) directly from the molecular dynamics settings. However, the homogeneity of the material as well as a simple cubic form of the domain was assumed. This makes such a method unsuitable in the case of materials containing defects. In order to address this issue, the coming section will present a procedure to extract heat conductivity in more general situations.

3. Heat conduction measure by response function analysis

One of the main goals of this work is to introduce a robust measure of the effective heat conduction when defects are introduced. For example, when only a fraction of an internal surface remains in contact the voids surrounding contacting asperities will restrain the total heat flux bringing a lower thermal contact conductance. As previously mentioned, the Green-Kubo statistics approach is unsuitable because of the local inhomogeneity. Also, the NEMD approach becomes extremely difficult since the geometrical bottlenecks will perturb the temperature gradient construction.

Thus, a direct approach is now proposed. It consists in measuring the temperature evolution when a heat impulse is imposed as a boundary condition. This temperature rise will be compared to its Fourier analytical prediction. Even though the physics involved at the atomistic scale differ from those represented by the Fourier heat equation, we will demonstrate in the following that the approach remains quite accurate. Let us consider a 1D bar of size L fitting in the range $[0, L]$. At initial time $t = 0$ the bar is considered at thermal equilibrium of temperature T_{init}. A Heaviside step of temperature T_{req} is applied to one edge of the bar while the other edge follows null thermal flux condition. Hence, the problem to solve can be expressed as:

$$\begin{aligned} \rho c_v \dot{T} &= -k \frac{\partial^2 T}{\partial^2 x} \qquad \forall x \in [0, L] \\ T(x, 0) &= T_{init} \\ \frac{\partial T(x,t)}{\partial x} \,|_{x=L} &= 0 \\ T(0, t) &= T_{req} \qquad \forall t > 0 \end{aligned} \tag{6}$$

A solution of the above problem can be found in [41] for the case where the heat conductivity is assumed constant. The temperature evolution follows:

$$T(L, t) = (T_{req} - T_{init}) \left(1 - \frac{4}{\pi} \sum_{p=0}^{\infty} \frac{(-1)^p}{2p+1} e^{-\alpha (\frac{(2p+1)\pi}{2L})^2 t} \right) + T_{init} \tag{7}$$

where α is the sought diffusivity. The obtained solution has the form of an infinite Fourier series with terms of decreasing magnitude with time forward.

In the context of molecular dynamics simulations, it is not clear yet whether the temperature evolution will follow the continuum diffusion equation since the discreteness of matter perturbs the heat transport, especially when small system sizes are considered. We used a molecular dynamics simulation with a plain block of atoms with dimensions $l \times l \times L$ with $L = 448a$ and $l = 24a$. This is a system containing $1,032,192$ atoms. The elongated geometry allows us to consider the problem as 1D. The equilibrium state at initial time is obtained by taking into account the thermal expansion described earlier concurrently with an initial set of Gaussian velocities. We relax the system, so as to obtain an adequate velocity distribution, with a Langevin thermostat at temperature 100 Kelvins which is applied on the entire set of atoms. Then the thermostat is changed to impose a temperature of 150 Kelvins on a thin layer of atoms at the bottom of the model. This creates the sought Heaviside boundary condition. Fixed atoms at the top of the domain provide the null heat flux boundary condition. The measure of the mean

kinetic energy with equipartition formula gives the temperature evolution with respect to time.

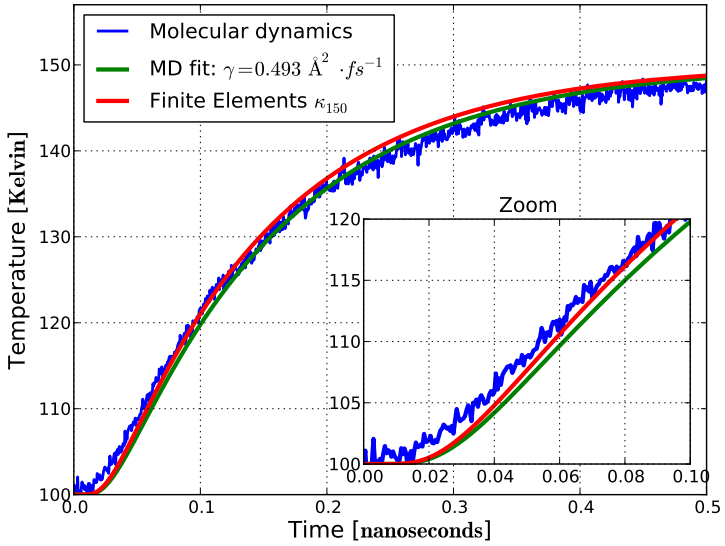

Figure 4: Temperature evolution resulting from a Heaviside change of temperature. Blue is the molecular dynamics result. The red curve represents the temperature evolution computed by solving Fourier equation with finite elements with the diffusivity set to k_{150} (value computed with the Green-Kubo approach). The green curve presents the best fit to the MD temperature evolution when using equation (7).

We wish now to compare temperature profiles with the analytical result of (7). The obtained record of temperature is foreground with the analytical prediction on figure 4. By fitting the MD temperature evolution to the equation (7), one can measure the diffusivity as $\alpha = 0.493$ Å^2/fs which leads to the conductivity value $k = 1.8 \cdot 10^{-4}$ kcal/mol/(fs $\cdot$ Å $\cdot$ K) when assuming constant capacity, which was observed in the studied range of temperature (see figure 2). The fitted curve is plotted in green on figure 4. This represents a small error $\frac{k-k_{150}}{k_{150}}$ of around 6% to the Green-Kubo prediction of k_{150}. The chosen jump of temperature $T_{req} - T_{init} = 50$ is an intermediate value, not too large, so that the Fourier prediction of (7) is not suffering inaccuracy from the variation of conductivity, and not too small, so that thermal noise is not polluting the curve fitting process.

In order to know the possible impact of using a Fourier model we performed a finite element simulation using the conductivity coefficient k_{150}. The finite element temperature evolution obtained is presented on Figure 4 as the red curve. It can be seen that the global trend is respected whereas the attention needs to be drawn to the onset of the temperature rise where molecular dynamics present a faster increase of temperature (see zoom in figure 4). Fourier theory does not reproduce the onset of temperature evolution which can be explained by the fact that the conductive bar has a finite size, constituted

of discrete atoms. This imposes that a part of the kinetic energy is transported at sound speed. This ballistic energy transport, is not taken into account by (7) since only Fourier heat equation is considered. This effect is expected to reduce with temperature increasing (acoustic waves disperse quicker with increasing thermal noise, a phenomenon known as phonon-phonon scattering). Also, much longer bars are expected to follow better our Fourier profile because the distance is another factor limiting the propagation of coherent acoustic waves. Unfortunately both of these physical arguments cannot easily be verified with the classical molecular dynamics tool because of the inter-atomic potential inaccuracy at high temperatures, and of the additional computational cost involved. On the other hand it is clear that the behavior at the beginning of the curve does not alter too importantly the measure of the conductivity done by curve fitting. We thus conclude that equation (7) is effective in determining thermal conductivity. This numerical approach will be used in the rest of the paper to characterize heat conductivity in the case of bars presenting defects. As a summary, table 1 shows the computed physical constants.

	Atomic units		SI units	
ϵ	2.4621	[kcal/mol]	$1.712 \cdot 10^{-20}$	[J]
σ	2.596	[Å]	$2.596 \cdot 10^{-10}$	[m]
r_{cut}	6.039	[Å]	$6.039 \cdot 10^{-10}$	[m]
m	26.98	[g/mol]	$4.4801 \cdot 10^{-26}$	[kg]
$a(T=0)$	4.0320	[Å]	$4.0320 \cdot 10^{-10}$	[m]
$a(T=100)$	4.04797	[Å]	$4.04797 \cdot 10^{-10}$	[m]
$\alpha_L(100<T<150)$	0.00396	[K^{-1}]	0.00396	[K^{-1}]
$\rho(T=0)$	1.65	[g/mol/Å^3]	2739.89	[kg/m^3]
$\rho(T=100)$	1.627	[g/mol/Å^3]	2701.7	[kg/m^3]
$c_v(100<T<150)$	$2.18987.10^{-4}$	[kcal/g/K]	916.85	[J/kg/K]
k_{100}	3.10^{-4}	[kcal/mol/fs/Å/K]	20	[W/m/K]
k_{150}	$1.9.10^{-4}$	[kcal/mol/fs/Å/K]	13.1	[W/m/K]
k_{fit}	$1.8.10^{-4}$	[kcal/mol/fs/Å/K]	12.2	[W/m/K]

Table 1: Summary table of the constants used for the MD and FE models.

4. Heat conduction through a contact interface

In order to study the conductivity through contacting asperities, we introduce defects with simple geometries so as to allow partial contact and thus partial heat transfer through the bar. Square asperities with steep borders are used for that purpose. Such an asperity is presented on the schematic of figure 5(a). In the domain considered, important regions are associated with tags (see 5(a)): temperature is measured in region 2, the thermostat is applied in region 5, regions 1 and 6 are fixed, and regions 3 and 4 are free of constraints. Around the asperities, the voids (hashed region on figure 5(a)) are filled with insulating (fixed) atoms. This insulating and rigid zone was introduced so that small asperities do not collapse because of thermal fluctuations as several of our attempts demonstrated (not presented here). Indeed the heating process creates a thermal expansion that can lead to important shear stresses in pillars of small sections.

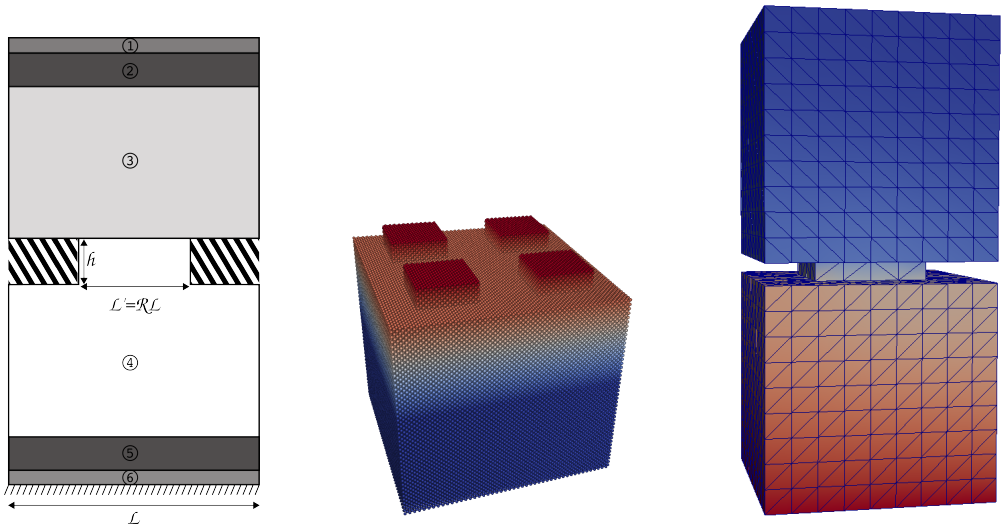

Figure 5: Schematic for the domain geometry which includes a single asperity (a), four asperities made of crystalline atoms (b), one single asperity made of finite elements (c). On (a), L stands for the width, h the length of the asperity and R is the contacting length ratio. For the upper body, the atoms into region 1 are fixed while in region 2 the temperature is monitored. The region 3 is free of constraints as well as the region 4 in the lower body. Region 5 is constrained to a Langevin thermostat and region 6 contains fixed atoms. The hashed regions are filled with insulating (fixed) atoms. On (b), only the bottom part is presented so that the asperity division process is illustrated. The dimensions are given by $L = 24$Å, $R = 0.5$, $h = r_{cut}$ and $D = 2$. The color scale used on (c) represents one temperature gradient typically obtained during continuum heat propagation simulations.

The model size L, the height of the crenel h, and the contact length ratio R are the three parameters which fully describe the domain shape when a single asperity is introduced. In order to study the influence of the asperity size without changing the global size (and thus the number of atoms) we also provided a division factor D that introduces D^2 asperities of area $(RL/D)^2$ each. This allows to decrease the asperity size while keeping the area of contact constant. An example of domain is presented for $L = 24a$, $R = 0.5$, $h = r_{cut}$ and $D = 2$ on figure 5(b). The Z-axis is normal to the contact surface. The usage of periodic boundary conditions on the sides of our box, ensures that we model an infinite surface.

Using the procedure described in the previous section, we conducted similar heat transport simulation in order to study the influence of the asperity size (i.e. wavelength) on the thermal contact conductance. In next section, the influence of the geometry parameters on molecular dynamics and finite elements heat propagation is sought.

4.1. Temperature evolutions

Figure 6(a) shows the effect of the contact area ratio on the MD temperature evolution in region 2 (see figure 5(a)) for a constant system size $L = 24a$. The temperature profiles follow an exponential shape with a time constant increasing for a decreasing contact ratio (a small contact area reduces the heat flux through the system, which

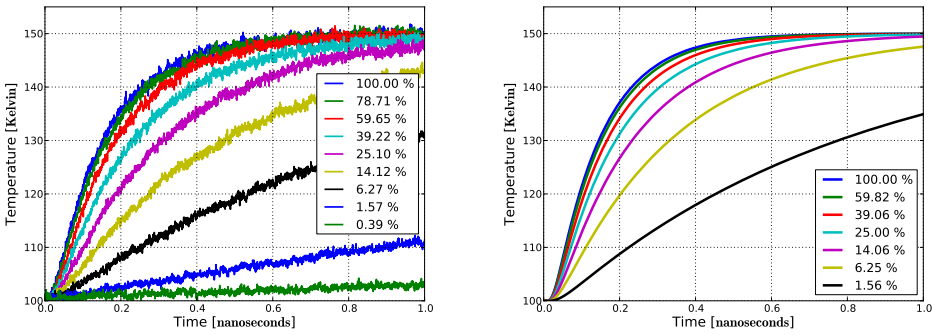

(a) (b)

Figure 6: Temperature evolution in region 2 (see figure 5a) for a system with section size $L = 24a$ and for various contact ratio: a) MD, b) FE.

delays the temperature rise). Figure 6(b) presents the obtained finite element analog. Finite elements curves are comparable to MD results even though time constants of exponential functions seem to differ substantially for the lowest contact ratios. Thus the measured conductivities will denote different trends as will be shown in the following section.

4.2. Thermal contact conductance

The effective conductivity has been extracted using equation (7) from the temperature profiles so as to exhibit the dependence to contact area ratio. Figure 7 shows the relative conductivity (k/k_0 with k_0 the conductivity for $A/A_0 = 1$) as a function of contact ratio, and this for asperities of several sizes. The single asperity finite element reference is also shown. The first observation is that the continuum Fourier heat equation does not provide the same trend as the molecular dynamics model. The main difference is brought by the slope at 0 % of contact. In the case of MD these slopes are all finite and not null, independently of the number of asperities. On the contrary, for the continuum calculations the slope looks infinite. This can be explained by the heat propagation nature being ballistic or diffusive.

When diffusive behavior is predominant, the scattering of phonons is not significant. This of course is the case when the scale of the asperity is large when compared to phonon's mean free path. Then, several analytical work predict a thermal contact conductance $k_d \sim \sqrt{A}$ [5]. In the ballistic regime, the corpuscular nature of phonons needs to be taken into account by including the scattering processes due to the interaction of phonons with boundaries of the contacting region. In that case Little [25] showed a relation of the form $k_b \sim A$. These two simple behaviors would lead to either infinite or finite slopes for diffusive and ballistic heat transport respectively. But it is clear from figure 7(a) that our atomistic model does not follow $k/k_0 \propto (A/A_0)^\beta$ - with $\beta \neq 1$ - be it for single asperity up to 49 asperities. This is probably due asperity interactions, which also come from periodic boundary conditions.

If the law directing contact conductance relations is a combination of diffusive and ballistic heat transport then it can explain the observed finite slopes. In the case of semi

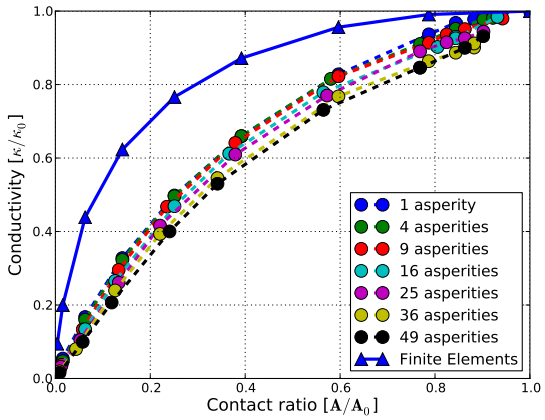

Figure 7: Relative conductivity with respect to contact area ratio for a domain of size $L = 24a$. The plain curves are obtained with a finite elements model whereas the dashed curves are obtained from molecular dynamics simulations. For these, the number of asperities where varied so as to present the influence of changing the per-asperity area to the global conductivity.

infinite domains for a single asperity, the work of Wexler [24], which used Boltzmann transport equation to enrich Little's formulas, allowed to introduce an interpolation term from ballistic regime to the diffusive-like behavior. Let us introduce a mixed behavior following:

$$k(x)/k_0(x) = \frac{1}{\alpha/x + \beta/\sqrt{(x)}} \tag{8}$$

where $x = A/A_0$, and α and β are the ballistic and diffusive contributions respectively. Fitting with a least square approach the above relation with the thermal conductance is providing figure 8(a). Even though the fit is not perfect (especially for FE), the trends are well represented. Furthermore, figure 8(b) shows that the diffusive contribution (resp. ballistic contribution) is decreased (resp. increased) when the scale of the asperity is diminished.

Because of the periodic boundary conditions, equation (8) cannot capture fully accurately our numerical results. Therefore, we considered a more generic shape which approximates satisfactorily the diffusion relations:

$$k(x)/k_0(x) = \frac{1}{ax^p + bx^q} \tag{9}$$

where a, b are two constants and p, q two exponents. Fitting this relation with the thermal conductance is providing a good approximation of the law in the MD and FE simulation cases as presented on figure 9(a). On figure 9(b) the fit coefficients and exponents are extracted for various numbers of asperities. It should be noticed that the sum of a and b coefficients is unity (within a numerical error) and have thus balanced effects. The parameter a (resp. b) decreases (resp. increases) when increasing the division parameter. The exponents show also variations with respect to the number of asperities making x^p evolve from $x^{-0.8}$ to $x^{-3/2}$ and x^q from $x^{0.7}$ to $x^{-0.39}$.

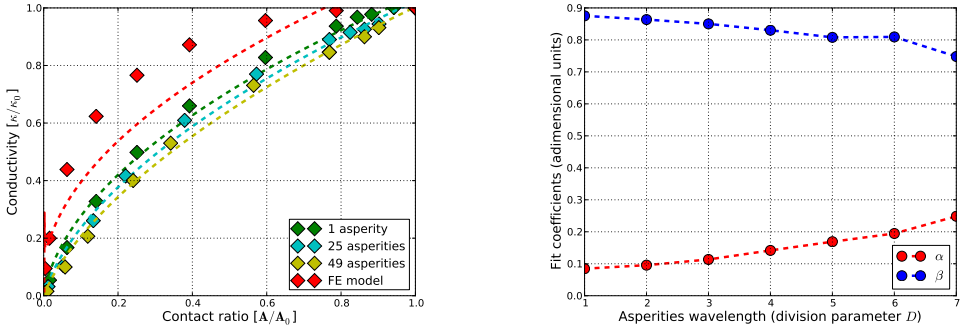

(a) (b)

Figure 8: (a) Thermal contact conductance with respect to contact area ratio. The diamond points are measures of the simulation runs using 1, 25 and 49 asperities. The dashed lines show the curves fitted from the analytical expression (8). (b) MD measure of the fit coefficients a and b which are the ballistic and diffusive contributions respectively. These coefficients are presented with respect to the division parameter D or equivalently to the wavelength of the surface.

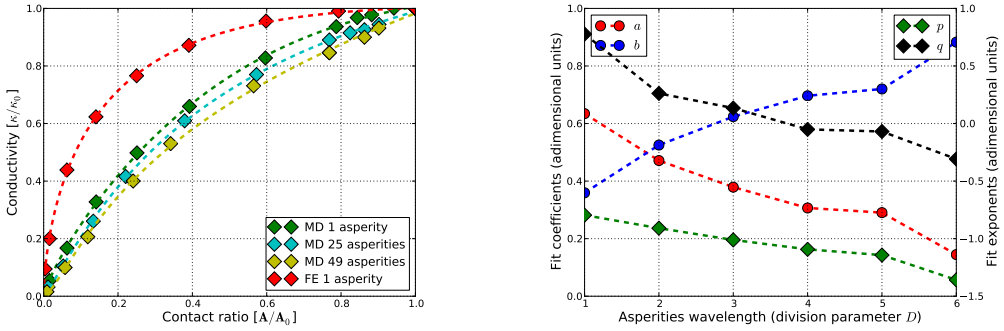

(a) (b)

Figure 9: (a) Thermal contact conductance with respect to contact area ratio. The diamond points are measures of the simulation runs using 1, 25 and 49 asperities. The dashed lines show the curves fitted from the analytical expression (9). (b) MD measure of the fit coefficients a and b and fit exponents p and q. These coefficients are presented with respect to the division parameter D or equivalently to the wavelength of the surface.

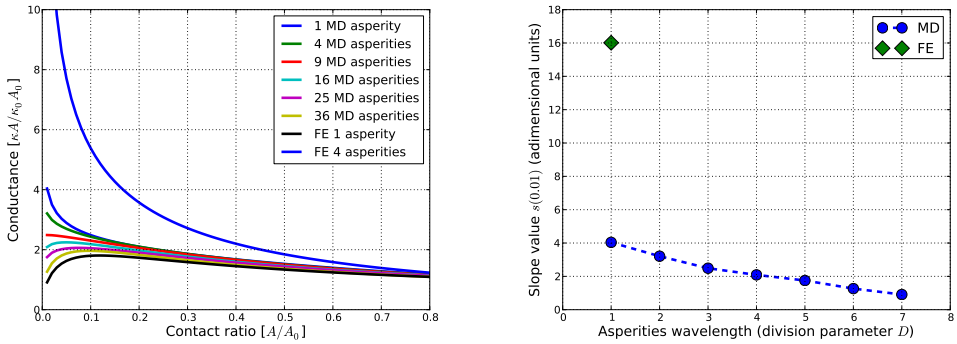

(a) (b)

Figure 10: (a) Slope function $s(x) = \frac{k(x)}{xk_0} = \frac{1}{ax^{p+1}+bx^{q+1}}$ plotted for FE and MD models for various number of asperities. (b) Value of $s(0.01)$ for the different geometry configurations for FE and MD models.

In the finite element case the fitted values provide:

$$k/k_0 = \frac{1}{0.58x^{-0.5} + 0.42x^{0.65}} \sim \frac{\sqrt{x}}{0.58} \quad when \quad x \to 0 \tag{10}$$

This is interesting since the square root shape provided by the analytical derivation of [5], which considered simple boundary conditions, is recovered asymptotically for a small contact area. Another interesting point is that the fitting process computed a non null coefficient b. Since the Fourier equation is solved in the FE case, b cannot represent a ballistic effect and is rather believed to be influenced by the boundary conditions.

The slope at small contact ratio is also interesting as it distinguishes the results for various numbers of asperity. We can define a *slope function* as the slope of the line connecting the origin point to any point x on the diffusivity curve. This leads to the expression:

$$s(x) = \frac{1}{x}\left(\frac{1}{ax^p + bx^q} - 0\right) = \frac{1}{ax^{p+1} + bx^{q+1}} \tag{11}$$

The function s is presented on figure 10 for which we can see a difference of behavior between MD and FE (scale effect), and between distinct number of asperities. The slope at the origin might diverge or converge depending on the number of asperities. This can be explained by computing the derivative of equation (9):

$$(k(x)/k_0)' = -\frac{ax^{p-1}p + bx^{q-1}q}{(ax^p + bx^q)^2} \sim -\frac{p}{a}x^{-p-1} \quad when \quad x \to 0 \tag{12}$$

The slope at the limit of zero contact area is finite only if $p < -1$, which is not always the case. This shows again that the global behavior is a combination between diffusion and ballistic regimes. Nevertheless if we decide a threshold of $A/A_0 = 0.01$ the values taken by s for all the ran simulation can be observed on figure 10(b). It is clear that the wavelength - or number of asperities - is influencing the initial slope which must have a correlation with phonon's mean free path. Thus parameters in equation (9) are

depending on the ballistic regime contribution. This point will need further investigation to establish correlations.

5. Conclusion

We computed the thermal contact conductance of surfaces characterized by cubic geometries of varying scales, in view of understanding the differences between atomic and continuum predictions of heat conduction. It is acknowledged that heat conductivity is difficult to determine. Classical methods cannot be used to compute thermal conductance of materials containing a localized defect as occurs at a contacting rough interface. An important contribution of our work is the development of a novel method that addresses this issue. Our approach is based on the analysis of the temperature profile from one edge of a solid due to a temperature impulse created at the opposite side. These profiles are then fitted to a predictive model based on the Fourier heat equation.

Finite element (FE) and molecular dynamics (MD) parametric studies have been conducted on a large set of contact surfaces where asperities sizes and global contact area ratio were varied. While generally both FE and MD display a similar trend for the variation of conduction as a function of the contact area ratio, we could observe clear distinct features. At small contact areas, the continuum simulation displays a strong variation (infinite) of conductance, which recalls the classical square root diffusion law. On the contrary, the atomistic scale shows smaller variation of the conductivity.

The different slopes at 0% contact area, observed while solving MD and FE, are recognized to belong to the ballistic and diffusive regime respectively. In the literature, the analytical approaches dealing with the conductivity through two objects joined by a small bridge, all consider semi-infinite geometries, which is not applicable for the present study. In order to characterize our observations, we parametrized the observed conductivity with a general equation providing good fits to our results. The slopes at the origin where contact vanishes have been computed allowing to establish a dependence to the number of asperities, or equivalently to the surface wavelength. It is tentative to think that the phonon scattering resistance to heat transfer could be related with this slope, introducing the idea that the gap of scales from atomistic to Fourier theory would be wavelength dependent.

For a real contact between random rough surfaces, the largest wavelength is acknowledged to contribute the most to the observable conductivity. Therefore, these results are interesting in the context of ultra-smooth non metallic surfaces for which the roughness belongs to the nanoscale. Then, the interactions between asperities may impact the conductivity because of ballistic effects.

Acknowledgments

This material is based on the work supported by the European Research Council Starting Grant no 240332. The authors would like to acknowledge useful discussions with Dr Vladislav Yastrebov and Dr Bernt Gotsmann.

Appendix A. Appendix: Temperature time-dependence Fourier solution to impulse stimulation.

Let us consider the problem as 1D, so that the differential equation to solve is written:

$$\frac{\partial T(x,t)}{\partial t} - \gamma \frac{\partial^2 T(x,t)}{\partial^2 x} = 0 \tag{A.1}$$

where γ is the heat diffusivity coefficient. The classical way to solve this *heat equation* is to consider the domain $[0, L]$ with boundary conditions fixing temperature $T(0) = T(L) = 0$. The method of separation of variables for the heat equation leads:

$$T(x,t) = A(x)B(t) \tag{A.2}$$

When introducing (A.2) in (A.1) we obtain the following relation:

$$\gamma \frac{A''(x)}{A(x)} = \frac{B'(t)}{B(t)} = -\nu \tag{A.3}$$

with ν a constant. Solving the first order differential equation acting on B leads to a first partial solution:

$$T(x,t) = e^{-\nu t} A(x) \tag{A.4}$$

leading to the family of solutions:

$$A(x) = C_1 cos(\omega x) + C_2 sin(\omega x) \tag{A.5}$$

By imposing the boundary conditions at initial time $T(0) = T(L) = 0$ we obtain that C_1 is zero. The admissible values of ω appear to be of the kind:

$$\omega_k = \frac{k\pi}{L} \tag{A.6}$$

Thus a family of A satisfying (A.3) is found:

$$A_k(x) = sin(\frac{k\pi x}{L}) \tag{A.7}$$

Inserting (A.7) into (A.3) we obtain $\nu = \gamma(\frac{k\pi}{L})^2$ so that the family (or generator) of solutions described above is

$$T(x,t) = e^{-\gamma(\frac{k\pi}{L})^2 t} sin(\frac{k\pi x}{L}) \tag{A.8}$$

Using the Fourier transform of the initial condition $T(x, 0)$, the general form of the solution is then

$$T(x,t) = \sum_k C_k sin(\frac{k\pi x}{L}) e^{-\gamma(\frac{k\pi}{L})^2 t} \tag{A.9}$$

This clearly states that the temperature variation depends on the frequency contributions to initial condition.

For the present study we wish to model a symetric problem with an impulse located at $x = 0$ and $x = L$ while the rest of the domain is at temperature $T_{req} = 1$. So that the initial condition can be defined by the function:

$$g(x) = \begin{cases} 0 & if x = 0 \ or \ x = L \ or \ x = -L \\ 1 & if x \in]0, L[\\ -1 & if x \in]-L, 0[\end{cases} \tag{A.10}$$

The Fourier coefficients are evaluated following the integral:

$$\begin{aligned} C_k &= \frac{1}{L}\int_{-L}^{L} g(x) sin(\frac{k\pi x}{L}) dx & \text{(A.11)} \\ &= \frac{2}{L}\int_{0}^{L} g(x) sin(\frac{k\pi x}{L}) dx & \text{(A.12)} \\ &= \frac{2}{L}\int_{0}^{L} sin(\frac{k\pi x}{L}) dx & \text{(A.13)} \\ &= \frac{2}{k\pi}\left(1 + (-1)^{k+1}\right) & \text{(A.14)} \end{aligned}$$

Only Fourier coefficients being odd are non zero so that we finally obtain:

$$g(x) = \frac{4}{\pi}\sum_{p=0}^{\infty} \frac{1}{2p+1} sin((2p+1)\frac{\pi x}{L}) \tag{A.15}$$

and the solution to our heat equation becomes:

$$T(x,t) = \frac{4}{\pi}\sum_{p=0}^{\infty} \frac{1}{2p+1} sin((2p+1)\frac{\pi x}{L}) e^{-\gamma(\frac{(2p+1)\pi}{L})^2 t} \tag{A.16}$$

For instance the value of the temperature at position $L/2$ verifies:

$$\begin{aligned} T(L/2,t) &= \frac{4}{\pi}\sum_{p=0}^{\infty} \frac{1}{2p+1} cos(p\pi) e^{-\gamma(\frac{(2p+1)\pi}{L})^2 t} & \text{(A.17)} \\ &= \frac{4}{\pi}\sum_{p=0}^{\infty} \frac{(-1)^p}{2p+1} e^{-\gamma(\frac{(2p+1)\pi}{L})^2 t} & \text{(A.18)} \\ & & \text{(A.19)} \end{aligned}$$

Since any linear combination of solution to the heat equation is also a solution (as long as the boundary conditions are well imposed) the function

$$\theta(x,t) = (T_{req} - T_{init})\,(1 - T(x,t)) + T_{init} \tag{A.20}$$

is solution of the heat equation with an initial condition having a zero temperature everywhere but for $x = 0$ and $x = L$ where the temperature is equal to T_{req} at all times.

References

[1] A. Shakouri. Nanoscale thermal transport and microrefrigerators on a chip. Proceedings of the IEEE, 94(8):1613 –1638, aug. 2006.

[2] P.R. Nayak. Random process model of rough surfaces. Journal of Lubrication Technology, 93:398, 1971.

[3] P.R. Nayak. Some aspects of surface-roughness measurement. Wear, 26:165–174, 1973.

[4] B.N.J Persson, O. Albohr, U. Tartaglino, A.I. Volokitin, and E. Tosatti. On the nature of surface roughness with application to contact mechanics, sealing, rubber friction and adhesion. Journal of Physics-Condensed Matter, 17(1):R1–R62, JAN 12 2005.

[5] M.G. Mikic B.B. Yovanovich M.M. Cooper. Thermal contact conductance. International Journal of Heat and Mass Transfer, 12(3):279–300, 1969.

[6] M.R. Yovanovich M.M. Sridhar. Elastoplastic contact conductance model for isotropic conforming rough surfaces and comparison with experiments. Journal of Heat Transfer, 118(1):3–9, 1996.

[7] M.M. Hegazy A.A. Antonetti V.W. Yovanovich. Experimental verification of contact conductance models based upon distributed surface micro-hardness. American Institute of Aeronautics and Astronautics, Aerospace Sciences Meeting, 1983.

[8] J.F. Molinari, M. Ortiz, R. Radovitzky, and E.A. Repetto. Finite-element modeling of dry sliding wear in metals. Engineering Computations, 18(3-4):592–609, 2001.

[9] P. Wriggers and C. Miehe. Contact constraints within coupled thermomechanical analysis–a finite element model. Computer Methods in Applied Mechanics and Engineering, 113(3-4):301–319, 1994.

[10] M. Culham J.R. Yovanovich M.M. Schneider G.E. Bahrami. Thermal contact resistance of non-conforming rough surfaces, part 2: Thermal model. Journal of Thermophysics and Heat Transfer, 18(2):218–227, 2004.

[11] M. Dibello S. Demelio G. Ciavarella. Conductance of rough random profiles. International Journal of Solids and Structures, 45(3-4):879–893, 2008.

[12] A.W. Gibson R.D. Bush. A theoretical investigation of thermal contact conductance. Applied Energy, 5(1):11–22, 1979.

[13] J.R. Barber. Bounds on the electrical resistance between contacting elastic rough bodies. Proceedings of the Royal Society A: Mathematical, Physical and Engineering Sciences, 459(2029):53–66, 2003.

[14] B.B. Mikić. Thermal contact conductance; theoretical considerations. International Journal of Heat and Mass Transfer, 17(2):205–214, 1974.

[15] A. Tevaarwerk J.L. Yovanovich M.M. Blahey. Contact Conductance Correlations of Elastically Deforming Flat Rough Surfaces, 1980.

[16] M. Paggi and J.R. Barber. Contact conductance of rough surfaces composed of modified rmd patches. International Journal of Heat and Mass Transfer, 54(21-22):4664 – 4672, 2011.

[17] J.F. Archard. Elastic deformation and the laws of friction. Proceedings of the Royal Society of London Series A-Mathematical and Physical Sciences, 243(1233):190–205, 1957.

[18] J. A. Greenwood and J. B. Williamson. Contact of nominally flat surfaces. Proceedings of the Royal Society of London Series A-Mathematical and Physical Sciences, 295:300, 1966.

[19] B. N. J. Persson. Theory of rubber friction and contact mechanics. Journal of Chemical Physics, 115:3840–3861, 2001.

[20] B. N. J. Persson. Contact mechanics for randomly rough surfaces. Surface Science Reports, 61:201–227, 2006.

[21] K. Charles. Introduction to solid state physics. Wiley, 1966.

[22] Z.M. Zhang. Nano/microscale heat transfer. McGraw-Hill Professional, 2007.

[23] A. Feher, A. A. Mamalui, A. Y. Dul'fan, E. S. Syrkin, and A. G. Shkorbatov. Low-temperature phonon transport in 3d point-contacts (review). Low Temperature Physics, 31:921–946, 2005.

[24] G. Wexler. Size effect and non-local boltzmann transport equation in orifice and disk geometry. Proceedings of the Physical Society of London, 89:927, 1966.

[25] W.A. Little. The transport of heat between dissimilar solids at low temperatures. Canadian Journal of Physics, 37:334–349, 1959.

[26] V. Varshney, J. Lee, A.K. Roy, and B.L. Farmer. Modeling of interface thermal conductance in longitudinally connected carbon nanotube junctions. Journal of Applied Physics, 109, 2011.

[27] D. Donadio and G. Galli. Temperature dependence of the thermal conductivity of thin silicon nanowires. Nano Letters, 10:847–851, 2010.

[28] L. Liu and X. Chen. Effect of surface roughness on thermal conductivity of silicon nanowires. Journal of Applied Physics, 107, 2010.

[29] P. Chantrenne and J. L. Barrat. Finite size effects in determination of thermal conductivities: Comparing molecular dynamics results with simple models. Journal of Heat Transfer-transactions of the ASME, 126:577–585, 2004.
[30] S. G. Volz and G. Chen. Molecular dynamics simulation of thermal conductivity of silicon nanowires. Applied Physics Letters, 75:2056–2058, 1999.
[31] M. R. Geller and K. R. Patton. Mesoscopic thermal transport through a weak link. Physica B-Condensed Matter, 316:445–447, 2002.
[32] Y. Dubi and M. Di Ventra. Colloquium: Heat flow and thermoelectricity in atomic and molecular junctions. Review of Modern Physics, 83(1):131–155, Mar 2011.
[33] R. Zwanzig. Non equilibrium Statistical Mechanics. Oxford University Press, 2001.
[34] F. Müller-Plathe. A simple nonequilibrium molecular dynamics method for calculating the thermal conductivity. Journal of Chemical Physics, 106(14):6082–6085, 1997.
[35] Hughes Thomas J.R. The Finite Element Method. John Wiley and Sons, 2001.
[36] T. Belytschko, W.K. Liu, and B. Moran. Nonlinear Finite Elements for Continua and Structures. John Wiley and Sons, 2001.
[37] M. P. Allen and D. J. Tildesley. Computer Simulation of Liquids. Oxford University Press, 1989.
[38] D. C. Rapaport. The art of Molecular Dynamics Simulation. Cambridge University Press, 1995.
[39] P. Spijker, G. Anciaux, and J.F. Molinari. The effect of loading on surface roughness at the atomistic level. Computational Mechanics, pages 1–11. 10.1007/s00466-011-0574-9.
[40] S. Yip. Handbook of materials modeling. Springer, 2005. p.766.
[41] H.S. Carslaw and J.C. Jaeger. Conduction of heat in solids. Oxford science publications, 1986.